galaxies

MDPI

Review

Consequences of Proton Acceleration in Blazar Jets

Apostolos Mastichiadis

Physics Department, National and Kapodistrian University of Athens, Athens 10679, Greece; amastich@phys.uoa.gr

Academic Editors: Jose L. Gómez, Alan P. Marscher and Svetlana G. Jorstad
Received: 5 September 2016; Accepted: 18 October 2016; Published: 2 November 2016

Abstract: Hadronic models of blazar emission constitute an interesting alternative to the more popular leptonic ones. Using the BL Lac object Mrk 421 as a characteristic example, we present two distinct ways of modeling the spectral energy distribution of blazars in the hadronic context, and we discuss the predictions of each variant on the spectral shape, the multi-wavelength variability, the cosmic-ray flux, and the high-energy neutrino emission. Focusing on the latter, we then present an application of the hadronic model to individual BL Lacs that were recently suggested to be the counterparts of some of the IceCube neutrinos.

Keywords: astroparticle physics; neutrinos; radiation mechanisms: non-thermal; galaxies: BL Lac objects

1. Introduction

High energy γ-ray observations have proven, beyond any doubt, that blazar jets can accelerate particles to ultrarelativistic energies. While it is quite possible that these particles are leptons, the hadronic origin of gamma-rays still remains an intriguing alternative, since this can have direct implications for both the sites of ultra-high-energy Cosmic Ray (UHECR) acceleration and for neutrino astronomy, especially in light of the recent IceCube detections [1]. In the present paper, we will present the consequences of the possible presence of ultrarelativistic protons in blazar jets. In Section 2, we will review the physical processes involved. In Section 3, we will discuss the basic variants of the hadronic model and the expected spectral and temporal signatures of each. We will also compare them to observations by using the nearby BL Lac object Mrk 421 as a characteristic example. In Section 4, we will adress the neutrino emission of the model, and we will discuss our results in Section 5.

2. Basic Principles

We will adopt the one-zone model for emission; i.e., we will assume that the region responsible for the blazar emission can be described as a spherical blob of radius R, containing a tangled magnetic field of strength B and moving towards us with a Doppler factor δ. We will further assume that high energy protons and (primary) electrons are injected uniformly throughout the volume of the blob. These will produce radiation via various physical processes, and thus a multiwavelength (MW) spectrum will be formed. All particles eventually are assumed to escape from the emitting region in a characteristic timescale, which can be equal to (or larger than) the photon crossing time of the source. This physical description assumes an ad hoc particle energization, but it can successfully treat the radiative transfer problem, which is complicated due to the many physical processes involved.

An emission model such as the above is defined as "leptohadronic"(or simply "hadronic") when the parameters of the emitting zone are such that the low-energy emission of the blazar spectral energy distribution (SED) is attributed to synchrotron radiation of primary electrons, while the observed high-energy (GeV–TeV) emission is of hadronic and not of leptonic origin.

While high energy electrons lose energy predominantly by synchrotron radiation and inverse Compton scattering, high energy protons lose energy through synchrotron radiation, photopair (Bethe–Heitler), and photopion production (see Figure 1 – note that processes that involve high energy interactions with matter, like relativistic bremmstrahlung and proton–proton collisions, are marginal, because the matter density in the jet is very low). Of these, photopion is the most complicated process, as it produces many unstable particles, such as pions ($\pi^{\pm}, \pi^0$), muons ($\mu^{\pm}$), and kaons ($K^{\pm}, K^0$), which then decay into lighter particles. For example, the decay of $\pi^{\pm}$ results in the injection of secondary relativistic electron–positron pairs ($\pi^+ \rightarrow \mu^+ + \nu_\mu$, $\mu^+ \rightarrow e^+ + \bar{\nu}_\mu + \nu_e$), while π^0 decay into very high energy (VHE) γ-rays. Therefore, photons and neutrinos, along with the injected protons and electrons (primary and secondary) can be considered as the stable populations that are at work in the blazar emitting region. Taking also into account that protons might turn into neutrons in photohadronic collisions, we can add neutrons as a stable population, since they are ultrarelativistic, and therefore their decay timescale (in the blob rest frame) is much longer than their escape timescale. (The charged pions and muons are assumed not to radiate. This can be justified from the fact that, for all relevant parameters, their decay timescales are much shorter than their synchrotron cooling timescales; therefore, their radiation has a negligible contribution to the emission of the region, while, at the same time, their production spectrum is not modified by losses.)

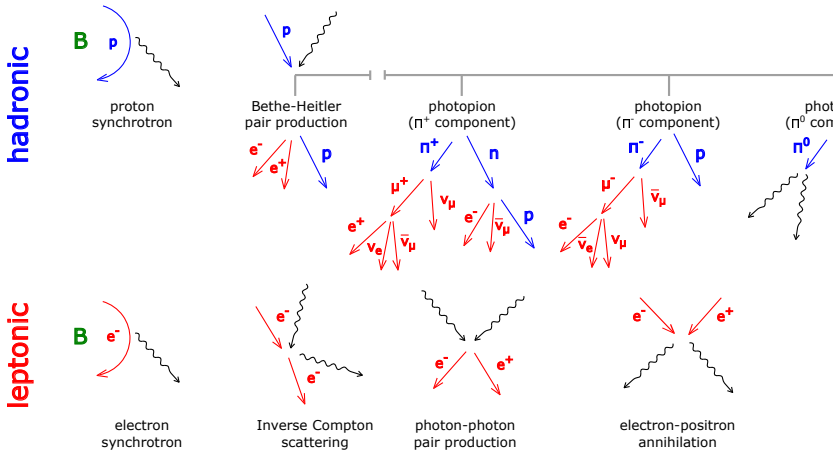

Figure 1. Schematic illustration of the main hadronic and leptonic processes that are included in our numerical treatment.

The three aforementioned hadronic processes act as energy loss mechanisms for protons, and as injection mechanisms for the other species. From these, only the modeling of proton synchrotron radiation can be considered straightforward. Photopair and photopion are non-trivial, and need careful modeling. For instance, one needs expressions both for proton energy losses and for the injection of the (stable) secondaries. For the former process, [2] used the Monte Carlo results of [3] to produce suitable distribution functions of the secondaries, and consequently to feed them in a kinetic type of equation. An analogous treatment was also followed for photopion. Here, the results of the event generator SOPHIA [4] were used in order to produce reaction rates for the secondaries [5]. We note that while Bethe–Heitler pair production has a contribution only to protons (losses) and electrons (gains) (in the present treatment positrons are treated identically to electrons), photopion contributes to all five stable species.

Having modeled the hadronic processes, one can follow the evolution of the distributions of the five stable particle populations with a set of five time-dependent, coupled partial integrodifferential kinetic equations, a treatment that allows energy conservation. In order to solve the system, we have used the numerical code of [6], augmented so as to incorporate the modeling of photopair and photopion interactions, as explained earlier. This has been described in detail in [5]. This treatment

has the advantage that it allows one to address topics such as the efficiency of proton luminosity conversion into photon and neutrino luminosities, the relation between their respective spectral shapes, as well as the stability of the system. As it was shown in [7], if the proton luminosity is above a critical value, the system can become unstable and show a limit cycle behaviour of the prey–predator type. This is a unique and interesting property of the hadronic models.

The input parameters of the code are related to the source characteristics, like the aforementioned R, B and δ, and to the specifics of particles injection, like their luminosity, the minima and maxima, as well as the slope of their distribution, assumed to be a power-law. As initial conditions, one can choose that the source has only a low number of protons and electrons that do not contribute significantly to the overall spectrum. Here, we assumed for simplicity that both distributions are initially equal to zero.

Once the parameters and initial conditions are specified, the system can be solved until some kind of steady state is achieved. This can occur when all parameters are kept constant in time and for low enough injected luminosities so as to avoid supercriticalities. The solution gives the proton and electron distribution functions, as well as the emerging photon, neutrino, and neutron spectra, which are all calculated simultaneously and self-consistently. Therefore, this approach has the great advantage that it can self-consistently normalize all particle distribution functions to the observed multiwavelength spectra of blazars, provided that reliablle fits to the MW spectra of the sources can be obtained. We also point out that the proton distribution function that one obtains from the solution does not need to be a power-law (even if the proton injection is a power-law), as it can exhibit breaks due to energy losses.

3. Hadronic Modeling of the BL Lac Object Mrk 421

Mrk 421 is one of the nearest ($z = 0.031$) and brightest BL Lac sources in the VHE ($E_\gamma > 200$ GeV) sky and extragalactic X-ray sky, which makes it an ideal target of multi-wavelength observing campaigns. Using Mrk 421 as our testbed, [8] found two acceptable ways of modeling the blazar SED in the hadronic context. In the first case, GeV and TeV $\gamma-$rays can be modeled through the radiation of photopion secondaries (the so-called LHπ model), and in the other through proton synchrotron radiation (the LHs model).

Table 1. Comparison of the hadronic model variants LHπ and LHs.

	LHπ model	**LHs model**
UV-to-X-rays	primary e^- synchrotron	primary e^- synchrotron
GeV-to-TeV γ-rays	secondary e^- synchrotron	p synchrotron
Dominant energy density	proton	magnetic
Jet power (erg/s)	$\sim 10^{48}$	$\sim 10^{46}$
Maximum proton energy	$\sim$20 PeV	$\sim$20 EeV
Maximum neutrino energy	$\sim$1 PeV	$\sim$1 EeV
X-ray flux vs. TeV flux	quadratic	linear

3.1. Photon, Neutrino and Cosmic Ray Spectra

Table 1 summarizes the main parameters of the two models concerning the photon, neutrino and UHECR spectrum expected. We give a brief discussion of these features below.

3.1.1. The LHπ Model

In the LHπ model (Figure 1, left panel) the photopion component is producing the observed γ-rays through synchrotron radiation of the electron–positron secondaries, which result from the $\pi^\pm$ decays and from the $\gamma\gamma$ absorption of the π^0 γ-rays [9]. The proton synchrotron component is suppressed as a result of a low magnetic field in combination with a high proton luminosity and a relatively low value of the maximum proton energy. It is interesting to note that despite the

fact that photopion is the dominant process, photopair leaves a very distinct signature on the MW spectra, as photopair produces very different secondary spectra than photopion (see Figure 4 of [5]). Therefore, despite the fact that it is less important energetically in the specific example, it produces non-overlapping spectra from the secondaries of photopion. Consequently the SED does not have the usual double-humped appearance, as synchrotron photons from the photopair secondaries produce a broad hump at MeV energies. This is so characteristic that we argue (Ref. [10]) that future detection of a third hump in the hard X-ray/soft $\gamma-$ray band that bridges the two usual ones but is lower in luminosity could be strong evidence for the LHπ model.

The energetic requirements of this model are high, while most of the energy is carried by the highest energy particles. Although the radiative efficiency of the model is low ($\sim 10^{-5}$), the high proton luminosity leads to a substantial neutrino flux that is of the same order as the TeV gamma rays. Interestingly, the expected $\nu_\mu + \bar{\nu}_\mu$ flux, which peaks at $\sim$3.3 PeV, is just under the sensitivity of the IC-40 detector (orange line). Detailed calculations (PCD) taking into account the neutrino flux when the source is flaring in photons suggest that Mrk 421 is a strong candidate for neutrino emission and should be detected within the next few years.

The cosmic-ray proton spectrum, on the other hand, results from neutron decay peaks at 70 PeV (Figure 1, right panel). This is just an upper limit of what it would appear at Earth, since we have not taken CR diffusion into account, which is important for energies $<10^{17}$ eV. At any rate, our values (even as an upper limit) are well below the observed CR flux at such energies; therefore, the LHπ model cannot account for it.

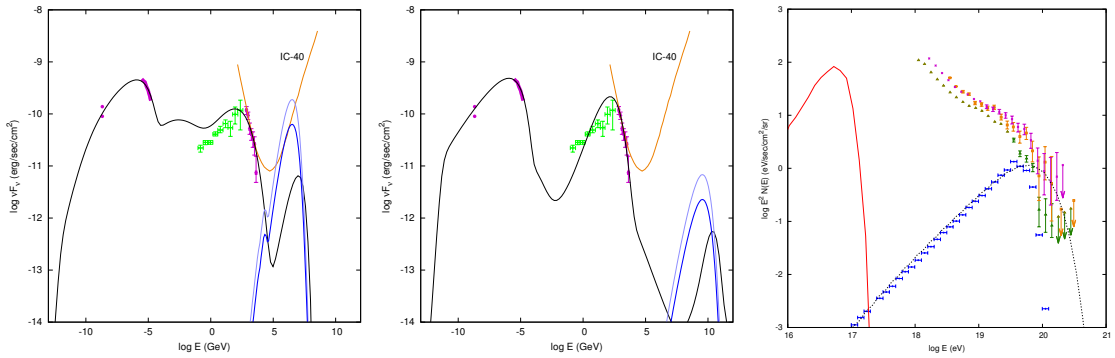

Figure 2. *Left* and *Middle* panels: spectra of photons (black line) fitting the March 22nd/23rd 2001 observation of Mrk 421 (purple points), neutrinos of all flavors (grey line), and $\nu_\mu + \bar{\nu}_\mu$ flux (thick blue line) according to the LHπ and the LHs models, respectively. Fermi observations (green points) are not simultaneous with the rest of the data, and are thus not included in the fit. The 40-String IceCube limit [11] for ν_μ is plotted with an orange line. *Right* panel: cosmic-ray (proton) spectra resulting from neutron decay and obtained within the LHπ (red line) and LHs (blue dashed line) models. For the latter, the cosmic-ray spectra obtained after taking into account propagation effects using the numerical code CRPropa 2.0 [12] are also shown (blue crosses). Different symbols are used for the cosmic-ray energy flux measurements by Auger, HiRes-I, and Telescope Array.

3.1.2. The LHs Model

The first ideas that proton synchrotron radiation can be responsible for the blazar γ-rays were put forward by Refs. [13,14]. In our variant of the the LHs model, the high magnetic field coupled with a low proton injection luminosity leads to a suppressed photohadronic component. The SED has two well-defined peaks, both from synchrotron radiation of electrons and protons at UV/X-rays and GeV/TeV γ-ray energies, respectively. This also results in a low neutrino flux (a factor of 10 less than the TeV γ-ray flux). The peak of the neutrino flux emerges at energies of $\sim$0.1 EeV, due to the high values of the magnetic field and of the maximum proton energy (see Table 1). The higher value of the maximum proton Lorentz factor used in the SED fitting makes the discussion about

ultra-high energy cosmic-ray (UHECR) emission more relevant. The propagation of UHE protons in a uniform intergalactic 1pG magnetic field and their energy losses from interactions with the cosmic microwave and infrared-optical backgrounds were modeled using CRPropa 2.0. The resulting spectra (blue crosses in right panel of Figure 2) peak at ∼60 EeV, and they are just below the present UHECR flux limits in the energy range 30–60 EeV.

3.2. *Variability*

The variability signatures expected in the framework of hadronic models have been studied in [15] by introducing small-amplitude variations to one (or more) model parameters around their time-averaged values. In particular, the temporal variations in the fitting parameter y were modeled as random-walk changes of the form $y_i \equiv y(t_i) = y_0\,(1 + 0.05\alpha_i)$, where $\alpha_{i+1} = \alpha_i + (-1)^\kappa$; here, κ is a uniformly distributed random integer number in the range (0,10). An indicative example is presented in Figure 3, where the varying model parameters are the proton and primary electron injection luminosities.

When the proton–electron variations are correlated, the LHπ model shows a quadratic relation between the TeV and X- ray fluxes, a behaviour that is very similar to the leptonic SSC model. Even in the cases where the proton–electron variations are uncorrelated, the X-ray and TeV γ-ray fluxes still keep a rather strong correlation. This can be explained from the fact that the primary electron-produced X-rays serve as targets for photo-pion interactions; therefore, the TeV γ-rays depend on both particles' distributions.

Contrary to that, in the LHs model, the X-ray–TeV correlation is present only in the case when the two variations of the two populations are correlated. When there is no correlation, the two fluxes also become uncorrelated. This is due to the fact that in the LHs model, TeV γ-rays are produced by proton synchrotron, and thus they do not depend in any way on the X-rays. Another difference is that a linear correlation of the two particle populations results in a linear correlation between the two fluxes.

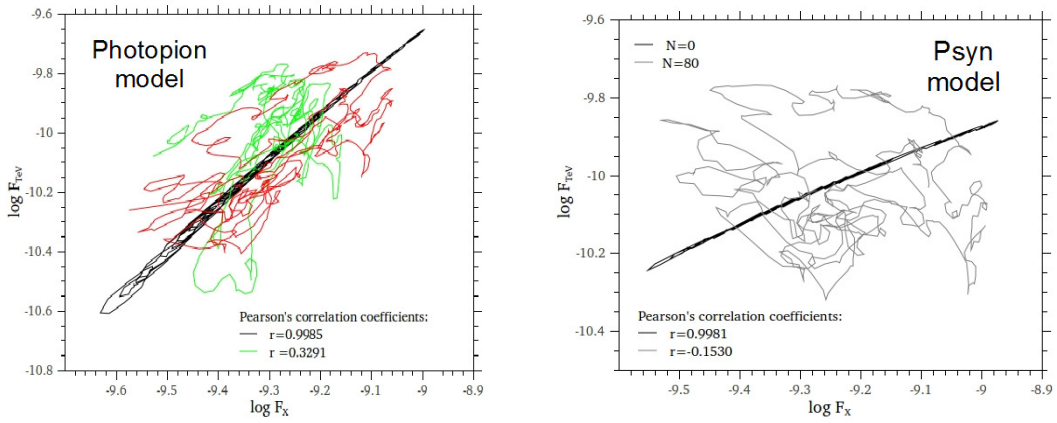

Figure 3. TeV γ-ray flux vs. X-ray flux as obtained in the LHπ (left panel) and LHs (right panel) models by varying the injection luminosity of primary electrons and protons. We considered the cases of uncorrelated variations (green line), as well as of correlated variations with no time-lag (black lines) and a positive time-lag of $80t_{\rm cr}$ (red and grey lines in the left and right panels, respectively).

4. Neutrino Emission from Individual BL Lacs

In [16], the authors have recently searched for plausible astrophysical counterparts within the median error circles of IceCube neutrinos using a model-independent method, and derived the most probable counterparts for 9 out of the 18 neutrino events of their sample. Interestingly, these include eight BL Lac objects (six with measured redshifts), amongst which the nearest are blazar, Mrk 421, and two pulsar wind nebulae. The (quasi)-simultaneous SEDs of those six BL Lacs, namely Mrk 421,

1ES 1011+496, PG 1553+113, H 2356−309, 1H 1914−194, and 1RXS J054357.3−553206, were fitted [17] with the leptohadronic model described in Section 2. The all-flavor neutrino fluxes derived by the model are presented in Figure 4.

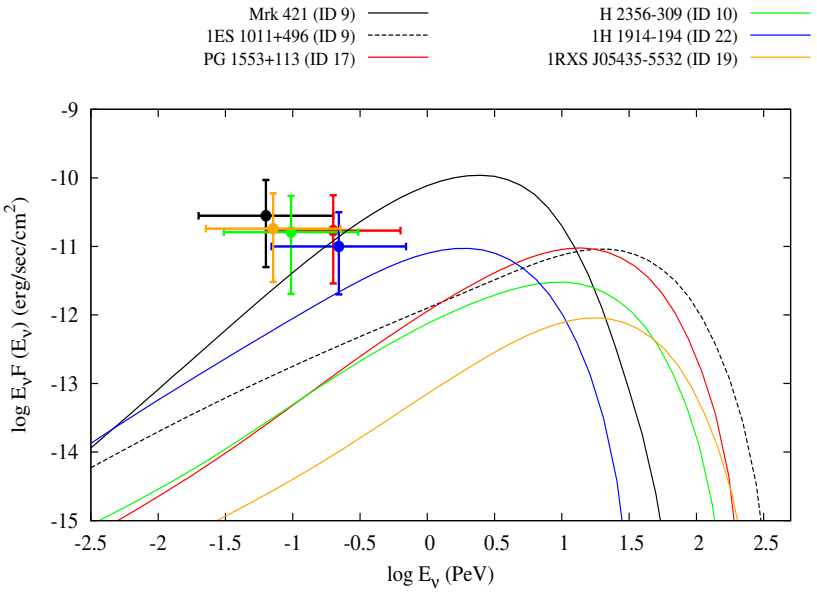

Figure 4. Comparison of the model (lines) and the observed (circles) neutrino fluxes as defined in [17] for the six BL Lacs of the sample. The Poissonian 1σ error bars for each event are also shown.

According to the model-independent analysis of [16], neutrino event nine has two plausible astrophysical counterparts: the BL Lacs Mrk 421 and 1ES 1011+496. The differences between the neutrino fluxes originate from the differences in their SEDs. In this regard, the case of neutrino event nine reveals in the best way how detailed information from the photon emission may be used to lift possible degeneracies between multiple astrophysical counterparts. As the neutrino spectrum for 1ES 1011+496 (dashed line in Figure 4) is an upper limit, our results strongly favor Mrk 421 against 1ES 1011+496.

In all cases, the model-derived neutrino flux at the energy bin of the detected neutrinos is below the 1σ error bars, but still within the 3σ error bars. Although the association of these sources cannot, strictly speaking, be excluded at the present time, blazars Mrk 421 and 1H 1914-194 are the two most interesting cases, because their association with the respective IceCube events can be either verified or disputed in the near future. Figure 4 demonstrates that the model-derived neutrino spectra from blazars with different properties are similar in shape. We may thus model the observed differential neutrino plus anti-neutrino ($\nu + \bar{\nu}$) flux of all flavors ($F_\nu(\epsilon_\nu)$) as $F_\nu(\epsilon_\nu) = F_0 \epsilon_\nu^\beta \exp\left(-\frac{\epsilon_\nu}{E_0}\right)$, where $\langle\beta\rangle \sim 0.34$ and E_0 is in good approximation equal to the peak energy of the neutrino spectrum, namely $\epsilon_{\nu,p}(\delta, z, \nu_s) \simeq 17.5\ \mathrm{PeV}(1+z)^{-2}\left(\delta/10\right)^2\left(10^{16}\mathrm{Hz}/\nu_s\right)$. In the above, δ is the Doppler factor, z is the source redshift, and ν_s is the *observed* synchrotron peak frequency. The luminosity from the photopion component is directly connected to that of ∼2–20 PeV neutrinos. Thus, our approach allows us to associate the observed blazar γ-ray flux with the expected all-flavor neutrino flux as $F_{\nu,\mathrm{tot}} = Y_{\nu\gamma} F_\gamma\,(> E_\gamma)$, where $E_\gamma = 10$ GeV and $Y_{\nu\gamma}$ is a factor that includes all the details about the efficiency of photopion interactions; for example, $Y_{\nu\gamma} \ll 1$ implies an SSC origin for the blazar γ-ray emission. The normalization F_0 can be then inferred from the above.

5. Discussion

Hadronic models for blazar emission assume that the observed GeV–TeV $\gamma-$rays are produced from interactions of high energy protons that have been accelerated in the jets of these objects. According to their basic premises, $\gamma-$rays can be produced either directly via proton synchrotron radiation (the LHs model) or via the synchrotron radiation of secondaries resulting from photopion interactions (the LHπ model). These ideas have been around for a long time (e.g., [9]). Careful modeling of the photo-hadronic processes ensures that at least the radiative transfer problem can be now treated adequately. This is done with the help of numerical codes (e.g., [5,18,19]) that take into account the many physical processes operating in such a system.

Hadronic models can fit the MW spectra of blazars [17,18,20] equally as well as the leptonic ones, albeit with a higher required jet luminosity—see [20]. This issue forms probably the most severe criticism of the hadronic models, and, according to some authors [21], might even require a change in the accretion paradigm. Interestingly enough, the energetics problem appears more severe for Flat Spectrum Radio Quasars (FSRQs) that require exceedingly high luminosities even after power minimization [22,23], while the situation might not be so severe for BL Lac objects [24].

Focusing on the case of BL Lac object Mkr 421, it is perhaps a little surprising that two hadronic models with very different parameters are able to produce good fits to the MW data. The more economic of the two, as far as jet power is concerned, is the LHs model—see Table 1. This model requires acceleration of protons to energies of tens of EeV, and it is magnetically dominated. Propagation of the proton produced from the escaping neutron decay results in a UHECR flux at Earth that is very close to the measurements of current experiments at energies around 30 EeV. However, due to the fact that our UHECR spectrum is peaked at high energies, its overall shape is very different from the observed one at energies below 30 EeV—see Figure 2, right panel. Even if one assumes that all other Northern Hemisphere nearby BL Lac objects produce the same spectral shape of UHECRs as Mrk 421 and normalize their cosmic-ray output to their photon luminosity, their contribution to the total UHECR flux will not be significant because of the combination of their low luminosities and of the cosmic-ray propagation through larger distances; we note that among these sources, Mrk 421 is not only the closest blazar, but also the most luminous one. Furthermore, the LHs model produces a low neutrino flux, since photohadronic processes are suppressed to a level that is many orders of magnitude below the IceCube sensitivity threshold—see Figure 2, middle panel. While it is possible to fit the SED with steeper proton injection spectra, we found that these cases cannot significantly alter our conclusions regarding UHECR and neutrino fluxes, as long as the injected power law index is less than 2.5. Concerning variability, the LHs model predicts a TeV γ-ray–X-ray flux correlation that simply mimicks the variability in primary electrons and protons (see Figure 3, right panel); i.e., the model is inherently linear. Therefore, any observed non-linearity in the two fluxes will require fine-tuning in the injection rates of electrons and protons.

The LHπ model, on the other hand, requires a large (but not unacceptable) jet power which is heavily particle-dominated. Good fits to the SED of the source are obtained, assuming that the protons are accelerated up to energies of the order of tens of PeV; therefore, they cannot contribute in any way to the UHECR flux. The inclusion of the Bethe–Heitler process in the modeling (a process that more often than not is ignored) results in a very characteristic low luminosity broad emission bump in the MeV regime that clearly separates the SED produced by the LHπ model from the SED produced by the LHs. The neutrino emission calculated by [8] is close to the current IceCube (IC-40) sensitivity limit for this source (left panel in Figure 3), and this was found a posteriori to be close to the observed flux related to neutrino ID 9. Therefore, PeV neutrino emission with a luminosity comparable to the TeV γ-ray emission is another feature of the LHπ model. Finally, simulated variability studies reveal that the TeV γ-ray–X-ray flux correlation is quadratic in the case where the electron–proton injection is linearly correlated. It is interesting that a rather strong correlation is retained in the fluxes even if the primary electron injection is totally uncorrelated with the proton injection.

6. Conclusions

In the last few years, hadronic models have become as sophisticated as the leptonic ones by including important physical processes, time-dependence, and self-consistency. They can fit the MW blazar observations, but they require—at least in the case of FSRQs—large jet power. They also can explain, in some variants, a non-linear correlation between X-ray and TeV γ-ray fluxes in agreement with observations. Finally, the expected neutrino flux is close to the recent IceCube detections, and probably it will be these types of detections that will ultimately probe the nature of high-energy radiating particles in blazar jets.

Conflicts of Interest: The author declares no conflict of interest.

References

1. Aartsen, M.G.; Ackermann, M.; Adams, J.; Aguilar, J.A.; Ahlers, M.; Ahrens, M.; Altmann, D.; Anderson, T.; Arguelles, C.; Arlen, T.C.; et al. Observation of High-Energy Astrophysical Neutrinos in Three Years of IceCube Data. *Phys. Rev. Lett.* **2014**, *113*, 101101.
2. Mastichiadis, A.; Protheroe, R.J.; Kirk, J.G. Spectral and temporal signatures of ultrarelativistic protons in compact sources. I. Effects of Bethe-Heitler pair production. *Astron. Astrophys.* **2005**, *433*, 765–776.
3. Protheroe, R.J.; Johnson, P.A. Propagation of ultrahigh energy protons and gamma rays over cosmological distances and implications for topological defect models. *Astropart. Phys.* **1996**, *4*, 253–269.
4. Mücke, A.; Engel, R.; Rachen, J.P.; Protheroe, R.J.; Stanev, T. Monte Carlo simulations of photohadronic processes in astrophysics. *Comput. Phys. Comm.* **2000**, *124*, 290–314.
5. Dimitrakoudis, S.; Mastichiadis, A.; Protheroe, R.J.; Reimer, A. The time-dependent one-zone hadronic model. First principles. *Astron. Astrophys.* **2012**, *546*, 120–132.
6. Mastichiadis, A.; Kirk, J.G. Self-consistent particle acceleration in Active Galactic Nuclei. *Astron. Astrophys.* **1995**, *295*, 613–628.
7. Petropoulou, M.; Mastichiadis, A. Temporal signatures of leptohadronic feedback mechanisms in compact sources. *Mon. Not. R. Astron. Soc.* **2012**, *421*, 2325–2341.
8. Dimitrakoudis, S.; Petropoulou, M.; Mastichiadis, A. Self-consistent neutrino and UHE cosmic-ray spectra from Mrk 421. *Astropart. Phys.* **2014**, *54*, 61–67.
9. Mannheim, K.; Biermann, P.L.; Krülls, W.M. A novel mechanism for nonthermal X-ray emission. *Astron. Astrophys.* **1991**, *251*, 723–731.
10. Petropoulou, M.; Mastichiadis, A. Bethe-Heitler emission in BL Lacs: Filling the gap between X-rays and γ-rays. *Mon. Not. R. Astron. Soc.* **2015**, *447*, 36–48.
11. Tchernin, C.; Aguilar, J.A.; Neronov, A.; Montaruli, T. An exploration of hadronic interactions in blazars using IceCube. *Astron. Astrophys.* **2013**, *555*, 70–83.
12. Kampert, K.-H.; Kulbartz, J.; Maccione, L.; Nierstenhoefer, N.; Schiffer, P.; Sigl, G.; van Vliet, A.R. CRPropa 2.0—A public framework for propagating high energy nuclei, secondary gamma rays and neutrinos. *Astropart. Phys.* **2013**, *42*, 41–51.
13. Aharonian, F. TeV gamma rays from BL Lac objects due to synchrotron radiation of extremely high energy protons. *New Astron.* **2000**, *5*, 377–395.
14. Mücke, A.; Protheroe, R.J. A proton synchrotron model for flaring in Markarian 501. *Astropart. Phys.* **2001**, *15*, 121–136.
15. Mastichiadis, A.; Petropoulou, M.; Dimitrakoudis, S. Mrk 421 as a case study for TeV and X-ray variability in leptohadronic models. *Mon. Not. R. Astron. Soc.* **2013**, *434*, 2684–2695.
16. Padovani, P.; Resconi, E. Are both BL Lacs and pulsar wind nebulae the astrophysical counterparts of IceCube neutrino events? *Mon. Not. R. Astron. Soc.* **2014**, *443*, 474–484.
17. Petropoulou, M.; Dimitrakoudis, S.; Padovani, P.; Mastichiadis, A.; Resconi, E. Photohadronic origin of γ-ray BL Lac emission: implications for IceCube neutrinos. *Mon. Not. R. Astron. Soc.* **2015**, *448*, 2412–2429.
18. Cerruti, M.; Zech, A.; Boisson, C.; Inoue, S. A hadronic origin of ultra-high-frequency peaked BL Lac objects. *Mon. Not. R. Astron. Soc.* **2015**, *448*, 910–927.
19. Diltz, C.; Böttcher, M.; Fossati, G. Time Dependent Hadronic Modeling of Flat Spectrum Radio Quasars. *Astrophys. J.* **2015**, *802*, 133–144.

20. Böttcher, M.; Reimer, A.; Sweeney, K.; Prakash, A. Leptonic and Hadronic Modeling of Fermi-detected Blazars. *Astrophys. J.* **2013**, *768*, 54–67.
21. Zdziarski, A.A.; Böttcher, M. Hadronic models of blazars require a change of the accretion paradigm. *Mon. Not. R. Astron. Soc.* **2015**, *450*, L21–L25.
22. Petropoulou, M.; Mastichiadis, A. On proton synchrotron blazar models: The case of quasar 3C 279. *Mon. Not. R. Astron. Soc.* **2012**, *426*, 462–472.
23. Petropoulou, M.; Dimitrakoudis, S. Constraints of flat spectrum radio quasars in the hadronic model: The case of 3C 273. *Mon. Not. R. Astron. Soc.* **2015**, *452*, 1303–1315.
24. Petropoulou, M.; Dermer, C.D. Properties of Blazar Jets Defined by an Economy of Power. *Astrophys. J. Lett.* **2016**, *825*, L11–L15.